Influence of Ag+ Interaction on 1D Droplet Array Spacing and the Repulsive Forces between Stimuli-Responsive Nanoemulsion Droplets

ARTICLE *in* LANGMUIR · SEPTEMBER 2014

Impact Factor: 4.46 · DOI: 10.1021/la5022802

2 AUTHORS:

John Philip
Indira Gandhi Centre for Atomic Research
179 PUBLICATIONS **3,176** CITATIONS
SEE PROFILE

Mahendran Vellaichamy
Indira Gandhi Centre for Atomic Research
26 PUBLICATIONS **102** CITATIONS
SEE PROFILE

Langmuir

Article

pubs.acs.org/Langmuir

Influence of Ag^+ Interaction on 1D Droplet Array Spacing and the Repulsive Forces between Stimuli-Responsive Nanoemulsion Droplets

V. Mahendran and John Philip*

SMARTS, Metallurgy and Materials Group, Indira Gandhi Centre for Atomic Research, Kalpakkam 603 102, Tamil Nadu, India

Supporting Information

ABSTRACT: This paper reports results on the effect of interaction of Ag^+ on 1D droplet array spacing and the repulsive forces between stimuli-responsive nanoemulsion droplets, stabilized with an anionic surfactant—sodium dodecyl sulfate—and a diblock polymer—poly(vinyl alcohol)−vinyl acetate. The repulsive interaction is probed by measuring the in-situ equilibrium force−distance in the presence of Ag^+ using the magnetic chaining technique. At a constant static magnetic field, emulsion droplets form 1D array that diffract visible light. A large blue-shift in the diffracted light is observed in the presence of interacting Ag^+ because of the reduction in the interdroplet spacing within the 1D array. The in-situ equilibrium force−distance measurement results show that the onset of repulsions and magnitude of repulsive forces are strongly influenced by the presence of Ag^+ in ppb levels. This suggests that the Ag^+ ions screen the surface charges through the formation of both Stern and diffuse electric double layer and produces a dramatic blue-shift in surfactant-stabilized emulsion, whereas a dramatic conformational change in the adsorbed polymer layer causes a reduction in the 1D array spacing in the diblock polymer stabilized emulsion. The force−distance results are compared with the predictions of electrical double-layer and repulsive steric forces. The droplet array shows an excellent selectivity to Ag^+ due to the strong interaction of Ag^+ with the stabilizing moieties at the oil−water interface. The possible mechanisms of interaction of Ag^+ with surfactant and polymer are discussed. The dramatic decrease in the 1D array spacing in the presence of Ag^+ may find promising practical applications in the development of optical sensors for selective detection of cations with ultrahigh sensitivity.

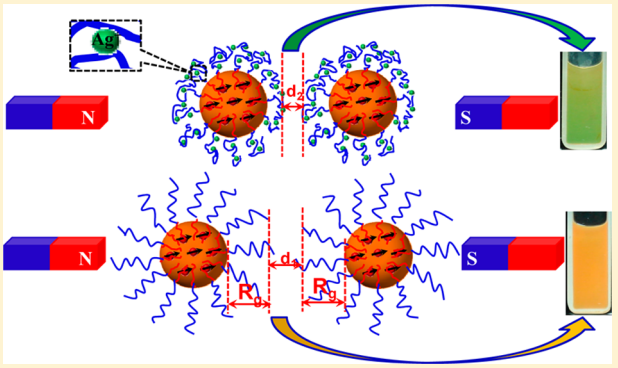

1. INTRODUCTION

Oil-in-water emulsions are used in many applications in food, cosmetic, pharmaceutical, and pesticide products.[1] Such emulsions are thermodynamically unstable but are made kinetically stable by employing suitable stabilization techniques such as electrostatic,[2] steric,[3,4] Pickering,[5,6] or a combination of the above.[7−9] An understanding on the interaction of stabilizing moieties (e.g., surfactants, polymers, nanoparticles, polyelectrolytes, and combination of these) with interfaces and the resulting forces between the colloidal droplets is very important in tailoring formulations with long-term stability.[10−12] Various force measurement tools have been used to assess the interaction between macroscopic surfaces and colloidal particles.[13−22] The stimuli-responsive materials (e.g., magnetic nanofluids,[23,24] magnetic nanoemulsions,[25] magnetorheological fluids,[26,27] photogelling fluids,[28] etc.) have been a topic of intense research in recent years because of their interesting properties and practical applications. Among various stimuli-responsive materials, magnetically responsive emulsions (popularly known as stimuli-responsive nanoemulsions) have been found to have several fascinating applications because of their ability to respond to a weak magnetic field and form various structures. In addition, they have been used as a model system to probe electrostatic, steric, electrosteric, and depletion interaction between emulsion droplets of size ranging from 100 to 200 nm.[15,29−31] Although electrostatic and steric interactions in colloidal system are well understood, the role of interfering species on interaction forces is unclear. The situation becomes more complex when the suspension contains ions of different valencies and ionic radii. In this paper, we probe the influence of cations at trace levels on the steric and electrostatic forces between the emulsion droplets and its consequence on the effective droplet spacing in stimuli-responsive nanoemulsions.

We chose Ag^+ as one of the main cations for our studies because silver nanoparticles have a multitude of applications in consumer and medical products owing to their antimicrobial properties. The oxidation and subsequent release of Ag^+ ions (soft Lewis acid) can cause disruption of cell growth, enzyme activities, membrane function, etc.[32] The tendency of these soft

Received: June 11, 2014
Revised: August 8, 2014
Published: August 8, 2014

ions to associate tightly with soft bases, such as the sulfhydryl groups, is believed to cause protein dysfunction or membrane damage,[33] and the antibacterial toxicity of soft metal ions is approximately proportional to their affinity for sulfur. Soft metals such as Ag^+, Cu^+, Hg^{2+}, Pb^{2+}, Cd^{2+}, Ni^{2+}, Zn^{2+}, and Co^{2+} have substantial affinities for protein thiols and are toxic to bacteria. The Ag^+ is known to associate with many other essential biologically important cations, thereby displacing or blocking their entry to cells.[34,35] Irrespective of intense studies, several questions on metal ion toxicity remain unanswered because of metabolic diversity of microorganisms (e.g., the route of entry of toxic metal ions to cells, modes of action of certain metal ions to key cellular processes, toxicity, etc.). Because of the toxic effect of Ag^+, it is important to have a highly sensitive and selective detection technique suitable for monitoring of Ag^+ in ppb levels. Although spectroscopic techniques such as atomic inductively coupled plasma mass spectroscopy and absorption or emission spectroscopy are well established methods, they are nonportable sophisticated equipment, expensive, and have poor selectivity in the presence of interfering ions because the signal from the other interfering species can often swamp the signal of the species of interest. Other electrochemical and optical techniques are also prone to cross-interference from various ions and lack ppb level sensitivity. This warrants the need to develop a simple, cost-effective, portable, and fast sensing device for selective and ultrasensitive detection of Ag^+. The second objective of our study was to explore the possibility of developing a sensitive optical technique for the selective detection of Ag^+ with high sensitivity using stimuli-responsive nanoemulsions. Toward realizing the above objectives, we probe the interaction of Ag^+ with the stimuli-responsive nanoemulsions and study its consequence on self-assembled nanoarray spacing by looking at the reflected Bragg peak positions.

The in-situ equilibrium force−distance measurements are carried out using magnetic chaining technique (MCT).[15] The MCT is a versatile, inexpensive, and easy to use tool suitable for probing interparticle forces such as screened electrostatic forces,[15] steric forces,[29,30,36] and electrosteric forces.[37] One of the important highlights of this technique is that the force measurement is based on averaging over an extremely large number of particles. We used a stimuli-responsive oil-in-water (O/W) nanoemulsion stabilized with an anionic surfactant—sodium dodecyl sulfate—or a diblock copolymer—poly(vinyl alcohol)-*co*-vinyl acetate—for our studies. The interaction of different cations such as K^+, Cu^{2+}, Ni^{2+}, Cd^{2+}, Mn^{2+}, and Pb^{2+} with the emulsion drops is also studied.

2. EXPERIMENTAL SECTION

2.1. Materials. The surfactant used was sodium dodecyl sulfate ($C_{12}H_{25}$-SO_4 Na), hereafter referred as SDS. The polymer used in the experiments was a statistical copolymer of vinyl alcohol−vinyl acetate (CH_2CHOH [88%]−$CH_2CH(OCOCH_3)$ [12%]), with an average molecular weight of 115 000 (referred as PVA-Vac 115K). PVA-Vac is a water-soluble polymer at room temperature, and its theta temperature in water is around 97 °C. The unperturbed radius of gyration (R_g) of the polymer was measured from viscosity measurements at a concentration well below the overlap concentration (C^*). In dilute concentration, viscosity follows the Einstein law $\eta/\eta_0 = 1 + 2.5\phi$, where η is the polymer solution viscosity, η_0 is the pure solvent viscosity, and ϕ is the coil volume fraction which is related to the hydrodynamic radius of the polymer.[36] The R_g of PVA-Vac measured by using viscometry is found to be ∼11 nm.

2.2. Emulsion Preparation. The stimuli-responsive magnetic nanoemulsion was prepared by shearing ferrofluid oil in the presence of an anionic surfactant and water using a homogenizer (IKA werke, T 25 Germany).[29] The Fe_3O_4 nanoparticles were synthesized by a coprecipitation method,[38] and the nanoparticles were characterized by techniques such as X-ray diffraction, transmission electron microscopy, thermogravimetry, Fourier transform infrared spectroscopy, and a vibrating sample magnetometer (Figure S1, Supporting Information). The ferrimagnetic Fe_3O_4 particle of size ∼10 nm sterically stabilized with oleic acid and dispersed in octane constitutes the oil phase. The crude emulsion was prepared by shearing ferrofluid oil, water, and surfactant in the ratio of 5:90:5. Later, the crude polydisperse emulsion was turned into a fairly monodispersed one by using fractionation technique.[39] Here, with excess surfactants, the larger emulsion droplets sediment first due to depletion flocculation induced by the nonadsorbed surfactant because of the uncompensated osmotic pressure. The depletion flocculation occurred at interdroplet separations smaller than the surfactant micellar diameter. To stabilize the emulsions electrostatically and sterically, SDS and PVA-Vac, respectively, were used. The amphiphilic character of these molecules facilitated the formation of a monolayer at the interface between water and the oil. The emulsion was washed with PVA-Vac (0.6 wt %) four times and incubated for 48 h before commencing the experiments. In the case of SDS stabilization, the emulsion was washed with SDS (0.8 mM) 3−4 times and used for further measurements.

2.3. Characterization of Magnetically Responsive Emulsions and Force Measurement. The hydrodynamic size and zeta potential of emulsions were measured using Zetasizer nano ZS (Malvern). A custom-made force apparatus has been used to probe the interdroplet force−distance curve.[37] An electromagnet with a programmable power supply is used to create a static magnetic field inside the sample. An AvaSpec-2048 fiber-optic spectrometer (Avantes, Netherlands) is used to obtain the Bragg peak position at different ion concentrations. The typical experimental setup used for the force−distance measurement is described Figure S2 (Supporting Information).[40]

2.4. Measurement of Spectral Response for Different Cations. To observe the effect of added cations on the interdroplet spacing, within the 1D array, about 200 μL of emulsion in a cylindrical vial was kept inside a solenoid coil, powered by a dc current source. The magnetic field inside the coil was fixed at 90 G. At this external field, magnetic dipole moments were induced in the oil droplets due to the alignment of the nanoparticles inside the droplet. The strength of the dipolar interaction is given by the coupling constant $\Lambda = \pi\mu_0 a^3 \chi^2 H_0^2/6k_BT$,[41] where a is droplet radius, χ is the magnetic susceptibility, H_0 is the external magnetic field, and k_BT is the thermal energy. Such dipolar interactions have been used to assemble colloidal particles into a variety of complex structures with dimensionality ranging from 0-D (rings) to 1-D (chains) to 2-D (tiles).[42] When the repulsive forces (electrostatic + steric) balance the field induced dipolar attraction, the droplets form a one-dimensionally ordered structure along the field direction. As the particle size is of the order of the wavelength of the visible light, each chain forms a lattice that diffracts light in the visible range, and the scattered light from each particle in the chain thus interferes constructively. The interdroplet spacing d for perfectly aligned droplets is related to the first-order Bragg condition (at 180° diffraction geometry) as $2d = \lambda_{max}/n$, where λ_{max} is the Bragg peak wavelength and n is the refractive index of carrier medium. For metal ions of different concentrations, the corresponding diffraction peak is recorded using a fiber-optic spectrometer. The Bragg peak without metal ions is taken as the reference peak. The shift in the peak wavelength with respect to the reference peak is called Bragg peak shift ($\Delta\lambda$). The change in the diffraction peak wavelengths with different metal cations of K^+, Cu^{2+}, Ni^{2+}, Pb^{2+}, Cd^{2+}, and Ag^+ are recorded, and the shift in the peak wavelength is calculated in each case.

3. RESULTS AND DISCUSSION

3.1. Properties of Magnetically Polarizable Nanoemulsion. Figure 1 shows the hydrodynamic size distribution

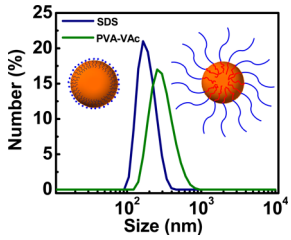

Figure 1. Hydrodynamic size distribution of magnetic nanoemulsion stabilized with SDS and PVA-Vac. Inset of the figures shows the schematic of droplet adsorbed with surfactant molecules and diblock copolymers. The average hydrodynamic size of SDS and PVA-Vac stabilized nanoemulsion are ~164 and ~255 nm, respectively. The corresponding zeta potential values are −41 and −1.8 mV, respectively.

of magnetic nanoemulsion stabilized with SDS and PVA-Vac. The inset of the Figure 1 shows the schematic of the droplet with adsorbed surfactant and diblock copolymer. The hydrophobic (Vac) part of the polymer prefers to remain inside the oil droplet, while the hydrophilic PVA part protrudes into the solvent to form a diffuse polymer layer. The average hydrodynamic sizes of SDS and PVA-Vac stabilized emulsions are found to be 164 and 255 nm, respectively, and the corresponding zeta potential values are −41 and −1.8 mV, respectively. The negative zeta potential value indicates the presence of negatively charged head groups (SO_4^-) at the oil−water interface, in the case of SDS stabilized emulsion. For PVA-Vac stabilized system, the very small value of zeta potential (−1.8 mV) indicates the presence of slight residual surface charges on the droplets, irrespective of repeated washing. The chemical structures of SDS and PVA-Vac are shown in Figure 2a,b. All our measurements are carried out

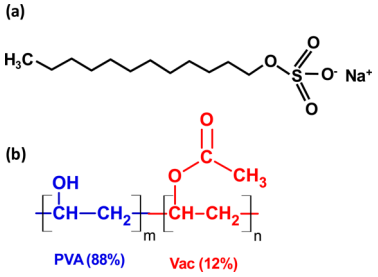

Figure 2. Chemical structure of (a) sodium dodecyl sulfate and (b) PVA-Vac.

from a master emulsion. The polydispersity of the emulsions was ~5%. Figure 3a,b shows the microscopic images of emulsions without and with an applied magnetic field, respectively. Figure 3c,d shows the schematic representation of the randomly distributed emulsion droplets without magnetic field and the aligned droplets along the direction of the applied magnetic field, respectively.

3.2. Effect of Ag^+ Interaction on 1D-Array Spacing.

Figure 4a shows the Bragg reflection spectra of an SDS stabilized nanoemulsion at various Ag^+ concentrations ranging from 0 to 525 ppb. In the absence of added cations, the diffraction peak occurs at 705 nm. The arrow indicates the direction of increasing concentration of Ag^+. It is observed that the Bragg reflection peak (λ_{max}) monotonically blue-shifts with increasing Ag^+ ion concentration, and the diffraction peaks are symmetric and narrow, inferring that the 1-D ordering is stable.

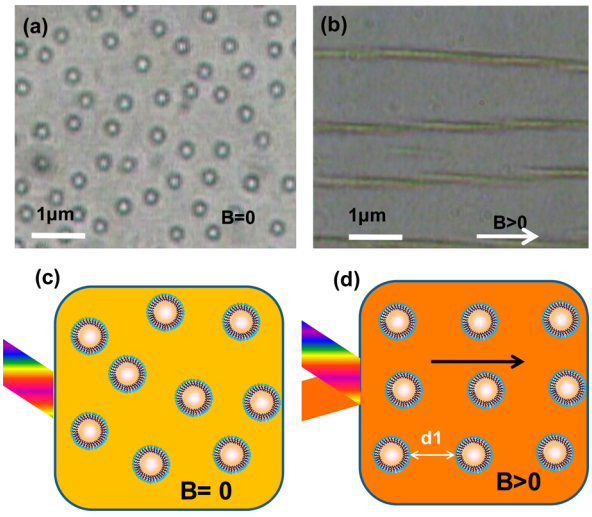

Figure 3. Microscopic images of emulsions (a) without and (b) with an applied magnetic field. Schematic representation of droplets configuration (c) without and (d) with an applied magnetic field. Direction of magnetic field is shown by an arrow.

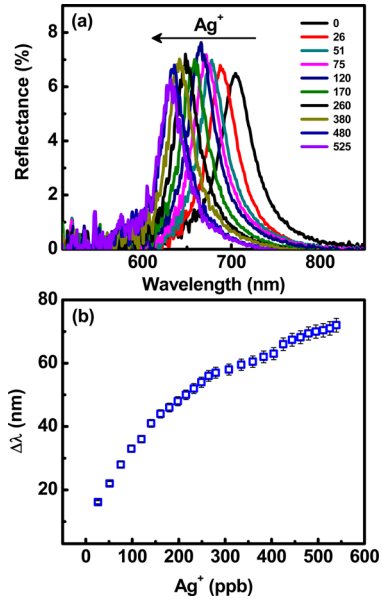

Figure 4. (a) Reflection Bragg spectra of an SDS stabilized emulsion at different Ag^+ concentrations. The arrow indicates the direction of increasing Ag^+ concentration. (b) Bragg reflection peak wavelength shift ($\Delta\lambda$) as a function of Ag^+ concentration for an SDS stabilized nanoemulsion.

Figure 4b shows the $\Delta\lambda$ as a function of Ag^+ concentration for SDS stabilized nanoemulsion. In the concentration range of 26−195 ppb, the observed linear slope value is 0.19, and above 195 ppb, the slope is 0.065. The higher slope indicates better sensitivity, and the slope change at higher concentrations indicates the change in sensitivity. Figure 5a shows the reflected Bragg peak observed for PVA-Vac stabilized emulsion at different Ag^+ concentrations. The arrow indicates the direction of increasing concentration of Ag^+. As observed in the case of SDS stabilized emulsion, the reflected Bragg peak monotonically blue-shifts on increasing Ag^+ ion concentration. Figure 5b shows the $\Delta\lambda$ as a function of Ag^+. The inset shows the concentration range (20−124 ppb) where the $\Delta\lambda$ is linear. The

dx.doi.org/10.1021/la5022802 | Langmuir 2014, 30, 10213−10220

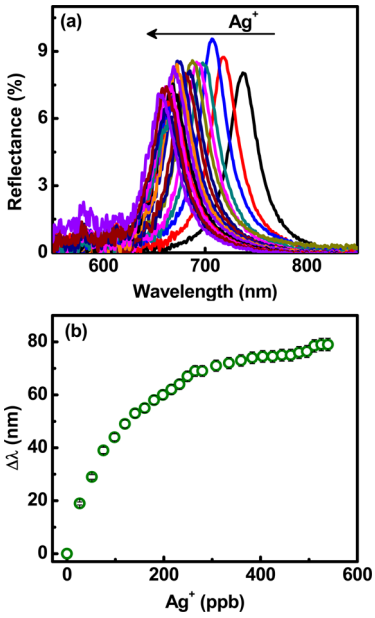

Figure 5. (a) Bragg reflection spectra of a PVA-Vac stabilized emulsion at different Ag^+ concentration. The arrow indicates the direction of increasing Ag^+ concentration. (b) $\Delta\lambda$ as a function of Ag^+ concentration.

slope of the linear fit and R^2 values are 0.32 and 0.97, respectively. Above 124 ppb, two different slopes are observed: one in the concentration range of 140−280 ppb and the second one for 300−490 ppb, and the corresponding slopes are 0.123 and 0.031, respectively. Figure 6 shows the $\Delta\lambda$ at different

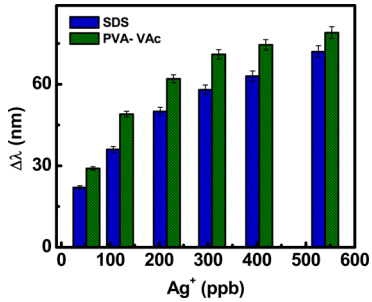

Figure 6. $\Delta\lambda$ at different concentrations of Ag^+ for SDS and PVA stabilized nanoemulsion.

concentrations of Ag^+ for SDS and PVA-Vac stabilized nanoemulsions. The average $\Delta\lambda$ value of PVA-Vac stabilized emulsion was ∼12 nm greater than that of SDS stabilized ones. This indicates that the PVA-Vac stabilized emulsion has a higher sensitivity to Ag^+ as compared to the SDS stabilized one. The possible reasons for the observed higher $\Delta\lambda$ in PVA stabilized emulsion is discussed in section 3.3. Figure 6 shows that the dynamic detection range of this approach is found to be 25−540 ppb.

To check the sensitivity of the emulsion to other cations, $\Delta\lambda$ measurements are carried out for SDS stabilized emulsion with different cations. The $\Delta\lambda$ variation is linear within certain concentration range for different cations. Figure 7a shows the $\Delta\lambda$ at 119.8 ppb of Ag^+ and 1 ppm of other cations for SDS stabilized nanoemulsion. The larger $\Delta\lambda$ for Ag^+ shows that the nanoemulsion has a better selectivity to Ag^+ compared to other cations used. To further evaluate the effect of interfering cations

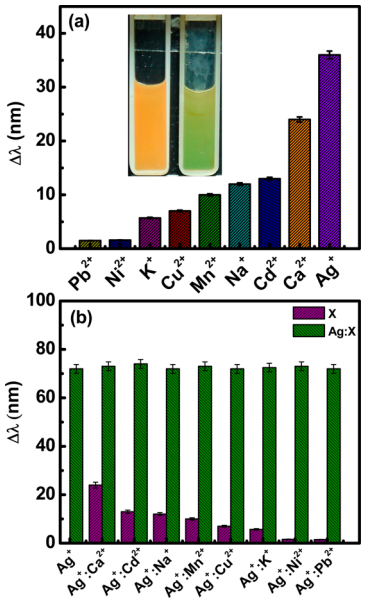

Figure 7. (a) $\Delta\lambda$ for SDS stabilized nanoemulsion at 119 ppb Ag^+ and for other cations at 1 ppm. Inset shows photograph of the emulsion without (left) and with 119 ppb of Ag^+ (right). (b) $\Delta\lambda$ for SDS stabilized nanoemulsion containing 539 ppb Ag^+ mixed with 1 ppm of different cations where X = Ca^{2+}, Cd^{2+}, Na^+, Mn^{2+}, Cu^{2+}, K^+, Ni^{2+}, and Pb^{2+}.

on detectibility of Ag^+, we have carried out experiments with a mixture containing Ag^+ and other cations (X) of higher concentrations. Figure 7b shows the $\Delta\lambda$ for different Ag^+:X ratios of 539 ppb:1 ppm. Without other interfering cations, for 539 ppb of Ag^+, the $\Delta\lambda$ was ∼70 nm. In the mixture with 1 ppm of Pb^{2+}, Ni^{2+}, K^+, Cu^{2+}, Mn^{2+}, Na^+, Cd^{2+}, and Ca^{2+}, the $\Delta\lambda$ is 1.5, 1.6, 5.7, 7, 10, 12, 13, and 24 nm, respectively. Even with 1 ppm of the interfering cations, the $\Delta\lambda$ remains nearly the same (∼70 nm). This clearly demonstrates the ultrahigh sensitivity and selectivity of this approach for Ag^+ detection. Among various cations, the maximum sensitivity (Bragg peak shift) is observed for Ag^+ ions. All these cations come under the soft acid group, which are acceptor atoms with a low positive charge and large size with several easily excited outer electrons. According to the hard−soft acid and base (HSAB) principle, soft acids prefer to coordinate with soft bases because electrons can be transferred readily either in one or both directions to form a covalent bond. The increasing $\Delta\lambda$ with the cations, followed the sequence $Pb^{2+} < Ni^{2+} < K^+ < Cu^{2+} < Mn^{2+} < Na^+ < Cd^{2+} < Ca^{2+} < Ag^+$. This trend can be partially understood on the basis of specific ion effects and the hydration of ions at interfaces.[43] Ag^+ is the softest acid among the studied cations, and the next softer cation is Cd^{2+}. Therefore, the observed order is in accordance with HASB theory. The exact reasons for the observed specific ion effect for Ag^+ requires further studies.

The situation becomes more complex as the specific ion effects on physicochemical properties of aqueous processes follow an empirical trend.[44] Further, the extent of interaction in Hofmeister cations depend not only on their hydration ability but also on the difference in size, polarizability, and effect on water structure. To the best of our knowledge, the range for Ag^+ in Hofmeister series is not reported in the literature. The Hofmeister sequence for (as salting-out agents in colloidal suspensions) anions and cations follows ($SO_4^{2-} > Cl^- > NO_3^-$) and $Na^+ > K^+ > Ca^{2+} > Ni^{2+} > Co^{2+}$, respectively.[45] However,

dx.doi.org/10.1021/la5022802 | Langmuir 2014, 30, 10213−10220

the above sequence is not exactly followed in our case, probably because of the associated anions. Earlier molecular dynamics simulation and X-ray absorption spectroscopic studies reveal that the hydrated Ca^{2+} cations can coordinate to oxygen atoms.[46] Further, it has been also shown that the solvated Ca^{2+} ion can wrap several oxygen atoms from the adsorbing species due the strong Coulombic attraction between Ca^{2+} ion and oxygen. Ag^{+} being the softest acid on the basis of this finding, a stronger interaction between the ions and oxygen from the PVA is anticipated, which would have resulted in a larger Bragg shift. Among the studied cations, Ag^{+} and Cd^{2+} are soft acids, Pb^{2+}, Cu^{2+}, and Ni^{2+} lie on the borderline, and K^{+} and Na^{+} are classified as hard acids.

3.3. Intermolecular Force Measurements. *3.3.1. Interaction of Ag^{+} with Electrostatically Stabilized Emulsions.* Figure 8a shows the force−distance profile for SDS stabilized

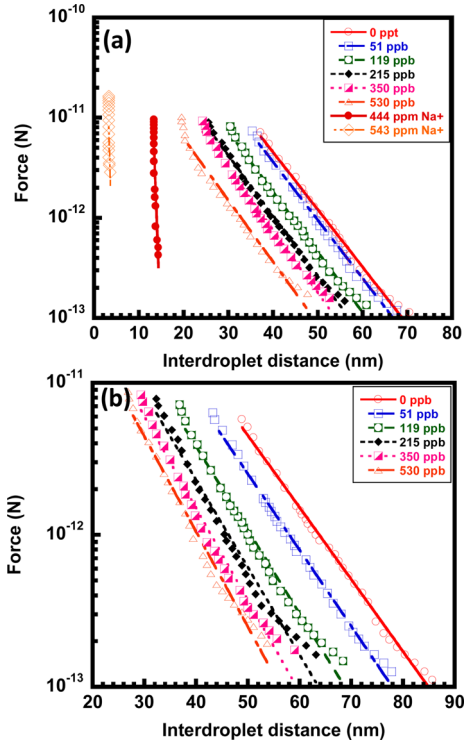

Figure 8. (a) Force−distance profiles at different Ag^{+} concentrations for SDS stabilized emulsion (scattered points). Solid lines correspond to fit using electrostatic double-layer repulsion equation. For comparison, force−distance profiles measured at 444 and 543 ppm of Na^{+} also shown. (b) Force−distance profiles at different Ag^{+} concentrations for PVA 115 K stabilized emulsion. Solid lines correspond to the theoretical fit to the force−distance profile.

nanoemulsion at different Ag^{+} concentration. The contribution of van der Waals attraction is also taken into the consideration while calculating the net force between droplets.[47] The SDS stabilized emulsions, without and with different Ag^{+} concentrations, show exponentially decaying repulsive force profiles. The decay length without Ag^{+} ion was 7.6 nm. Owing to the amphiphilic nature, SDS molecules adsorb at the droplet surface with the negatively charged headgroup exposed to water, thereby making the droplets negatively charged. The co-ions with negative charge and the counterions with positive charge form an electric double layer.[48] The chemical potential of counterions in the solution is given by $\mu = ze\psi + kT \log \rho$, where ψ is the electrostatic potential, e is the electron charge, z is the valency of ions, and ρ is the number density of ions at any point in the double layer. At lower surface charge densities the counterion becomes diffuse;[49] cations diffuse into a weak double layer and affect the strength of repulsion and the interdroplet spacing. According to electrical double layer theory, the repulsive force profile for $\kappa a < 5$ is $F_r(r) = 4\pi\varepsilon\psi_0^2 a^2[\kappa/r + 1/r^2] \exp[-\kappa(r - 2a)]$ and for thin electrical double layers with $\kappa a > 5$ the Derjaguin approximation with ψ remains constant and independent of $h = r - 2a$; the force profile can be represented as $F_r(r) = 2\pi\varepsilon\psi_0^2 ak\{\exp[-\kappa(r - 2a)]/[1 + \exp[-\kappa(r - 2a)]]\}$,[15] where a is the droplet radius, r is the droplet separation distance, ε is the dielectric permittivity of the suspending medium, ψ_0 is the electrical surface potential, and κ is the inverse Debye length. The best fit on the experimental data points using this equation is shown by the solid line. From the force−distance profiles, we obtain three parameters: the first interaction length ($2L_0$) that corresponds to the interdroplet spacing at a force magnitude of 2.8×10^{-13} N, decay length (κ^{-1}) from the slope, and the magnitude of force (K), which is dictated by the surface potential or the adsorbed polymer layer. The variation of these three parameters as a function Ag^{+} concentration for SDS (solid symbols) is shown in Figure 9a−c.

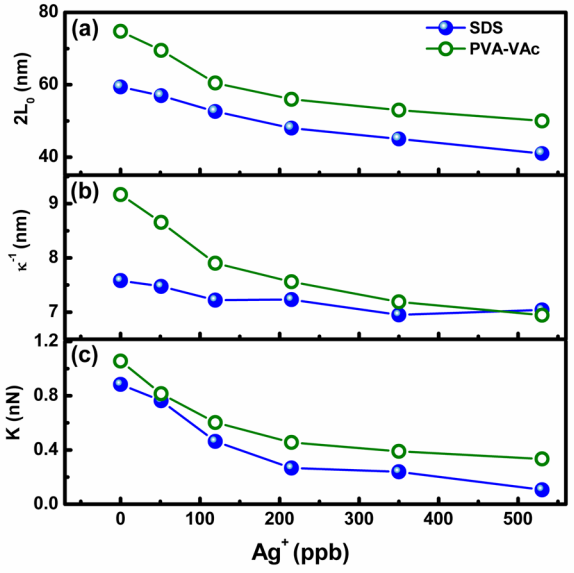

Figure 9. (a) First interaction length ($2L_0$), (b) Debye length (κ^{-1}), and (c) magnitude of force (K) for SDS and PVA stabilized emulsion as a function of Ag^{+} concentration.

The force−distance results suggest that the Ag^{+} ions, even at very low concentration, screen the charges at the emulsion surface probably through the formation of both Stern and diffuse electric double layers. The theoretical Debye length ($\kappa^{-1} = (1/4\pi)[2L_B^2 C_s]^{-0.5}$, where C_s is the electrolyte concentration and L_B is the Bjerrum length[49]) for 0.8 mM SDS stabilized system is 10 nm, which is in reasonable agreement with the value obtained from the best fit (~7.6 nm). The Debye length almost remains the same (~7.1 nm) for all the curves, irrespective of the concentration of Ag^{+}. This is quite expected because the concentration of SDS was much higher compared to that of Ag^{+}, and hence the effective decay length is dictated by SDS ions. Calculation shows that the number of SDS and

dx.doi.org/10.1021/la5022802 | Langmuir 2014, 30, 10213−10220

Ag^+ are 4.8184×10^{20} and 3.011×10^{18} for 0.8 mM SDS and 539 ppb Ag^+, respectively. As the decay length remains almost constant, the bound Stern layer contribution seems to play a prominent role in the charge screening process and hence the blue-shift. The strong interaction between Ag^+ (a soft Lewis acid) and RSO_4^- group of the surfactant is expected to cause abrupt changes in the magnitude of force. Such a strong association between soft acid and soft base is predicted by the Pearson's acid base theory.[50] The surface potential (calculated from the preexponential factor of the force−distance profile) with different Ag^+ concentrations is varying from 14.11 to 4.9 mV. For comparison of decay length variation, the force profiles with 444 and 543 ppm of Na^+ ions are also included in Figure 8a. It can be seen that the force profiles show a hard sphere profile at high concentrations of Na^+ because of screening of surface potential. The three possible modes of interaction of SDS with Ag^+ ions are the direct binding of Ag^+ to SDS, hydrated Ag^+ sharing one water molecule with the SDS, or Ag^+ interacting with the SDS via two water molecules (Supporting Information).

3.3.2. Interaction of Ag^+ with Sterically Stabilized Emulsions. The force−distance profiles (Figure 8b) of PVA-Vac stabilized nanoemulsion with different Ag^+ concentrations also show exponentially decaying nature. The zeta potential of PVA-Vac stabilized emulsions (−1.8 mV) indicates that there are some residual charges at the oil interface even after the washing process. However, the observed decay length of 9.2 nm (comparable to R_g of the polymer) clearly indicates that the droplet interface is covered by polymer where steric force is significant. Otherwise, the decay length would have been much higher. Without and with different Ag^+ concentrations, the repulsive force profiles are exponentially decaying. Here, the observed force profile arises from the repulsive osmotic force due to the unfavorable entropy associated with the compression of chains between the droplet surfaces.[3,49] According to Alexander−de Gennes equation[51,52] for polymeric brush bearing surfaces, the osmotic repulsion between the coils favors their expansion that can lead to an increase in $2L_0$, and the elastic stretch energy of the chains can favor a contraction or a decrease in $2L_0$. Of course, the steric forces are complex and depend on the surface coverage, nature of binding (physisorption or grafting with functional moieties), and the quality of solvent. In the present case, the physisorbed PVA coils bind reversibly at a number of points on the droplet interface where the adsorbed layers are highly dynamic, and hence the measured forces can be time dependent and history dependent, approach or separation rate dependent, or hysteretic.[49] However, our studies shows that incubation for a period of >48 h is sufficient to achieve an equilibrium binding of the polymers where the force profiles are found to be time independent and nonhysteretic. Studies reveal various interesting scenario when polymer or surfactant or both interact with an interface.[53,54] The variation of $2L_0$, characteristic decay length, and K as a function Ag^+ concentrations for PVA-Vac (open symbols) are shown in Figure 9a−c.

With the addition of 539 ppb of Ag^+, the $2L_0$ decreases from 72 to 52 nm, and the magnitude of force falls by an order from 5.9 to 0.59 nN. For polymer covered emulsion droplets, the force profiles are repulsive in nature and follow a simple exponential function $F(r) = k \exp(-h/\lambda)$, where r is the interdroplet spacing, λ is the decay length, and $k = k_B T \pi a/\lambda^2$, where k_B is the Boltzmann constant, a is the radius of the spherical droplets, and T is the temperature. Without added cations, the observed λ value is comparable to the radius of gyration of a free polymer (~12 nm). At a distance larger than λ, the concentration is dominated by the tails where the force is repulsive and decays exponentially with the distance. The increased osmotic pressure between the surfaces due to the overlap of adsorbed polymers leads to a repulsive interaction. It is known that the magnitude and range of steric forces can be many times R_g (>$10R_g$ in aqueous solutions) due to a high polymer surface coverage, higher Flory radius due to segment−segment repulsion (in good solvents), hydration layers, or additional repulsive electrostatic interactions between charged segments.[55]

With increasing Ag^+ concentration, the decay length decreases marginally from 9.1 to 6.8 nm, but the $2L_0$ decreases drastically from 74.8 to 50 nm. This shows a dramatic conformational change in the adsorbed polymer layer at the droplet interface. The decrease in the first interaction length indicates a collapse of stretched tail regions. Such a collapse is observed with the addition of salt in polyelectrolytes and under poor solvent conditions.[56] Further, the magnitude of the repulsive force decreases from 1.06 to 0.34 nN, as the concentration of Ag^+ is increased from 0 to 539 ppb. The mean field approach[42] distinguishes loops and tail sections in the adsorbed chains and involves the adsorbed layer thickness λ and an adsorption length z^* that separates the regions. The monomer concentration is dominated by loops, tails, and a microscopic length b inversely proportional to the adsorption strength. According to the mean field approach, in the strong adsorption limit ($\lambda/b \gg 1$), the adsorbed layer thickness is proportional to R_g and weakly dependent on the adsorption strength and polymer concentration. At a distance larger than λ, the concentration is dominated by tails, and the force is expected to be repulsive and exponentially decaying. The interaction of cations with PVA-Vac can lead to three possible modes of interactions: the direct binding of cations to the oxygen in the PVA-Vac chains, hydrated cations sharing one water molecule with the polymer, and cations interacting with the polymer via two water molecules.[57] The strongly hydrated Ag^+ [58,59] is expected to bind with the hydrophilic part of PVA-Vac by changing the entropy of hydration of water around the polymer using one of the mechanisms discussed above. Three possible interactions of OH of PVA and Ag^+ molecules are shown in Figure 10a. Figure 10b shows the schematic of the conformation of PVA-Ag^+ at the droplet interface. The variation of $2L_0$ in the presence of Ag^+ in SDS (Figure 10c) and PVA-Vac (Figure 10d) stabilized droplet is shown schematically. More systematic simulation and experimental studies are necessary to fully unravel the observed specific ion effect.

A molecular dynamics simulation study shows that the hydrated cations can be wrapped by seven oxygen atoms from three PVA-Vac chains due to the strong Coulombic attraction between cations and oxygen which tends to entangle or bridge segments of the chains together.[46] The observed dramatic reduction in the $2L_0$ value with increasing Ag^+ concentration is in line with the simulation predictions. The interaction of Ag^+ with the polymer by two water molecules in their first hydration shell, compared to a single water molecule or direct interaction by Ag^+, is expected to cause maximum conformational changes in the adsorbed tail regions of the PVA, as shown schematically in Figure 10d.

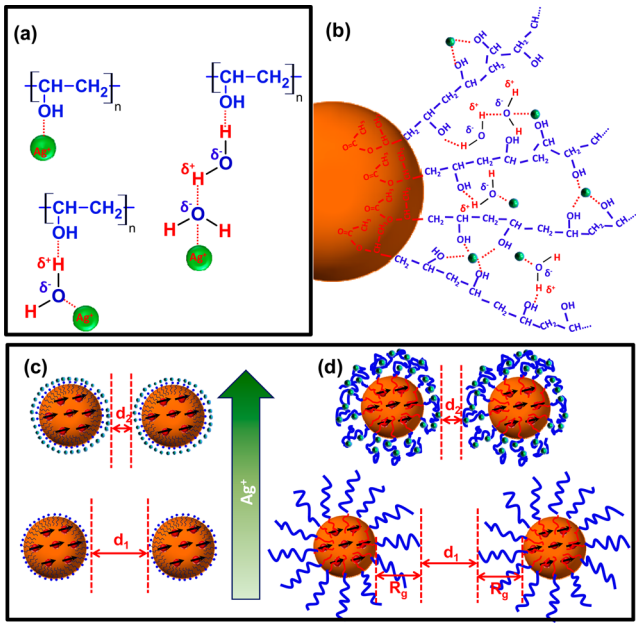

Figure 10. (a) Possible interaction of OH of PVA and Ag^+ molecules and (b) schematic of the conformation of PVA-Ag^+ at the droplet interface. Schematic representation of the interdroplet spacing variation in the presence of Ag^+ for (c) SDS and (d) PVA-Vac stabilized droplets and their conformation.

4. CONCLUSIONS

We studied the effect of Ag^+ interaction on 1-dimensional interdroplet array spacing and the electrostatic and steric forces between stimuli-responsive nanoemulsions. We observed a large blue-shift in the diffracted light because of the reduction in the interdroplet spacing in the presence of interacting Ag^+. The order of increasing of Bragg peak shift for different cations followed a sequence $Pb^{2+} < Ni^{2+} < K^+ < Cu^{2+} < Mn^{2+} < Na^+ < Cd^{2+} < Ca^{2+} < Ag^+$. The in-situ equilibrium force−distance measurement results suggest that the Ag^+ ions screen the charges at emulsion surface through the formation of both Stern and diffuse electric double layer and produce a dramatic blue-shift. In the presence of interfering cations, excellent selectivity is observed for Ag^+ due to strong interaction of hydrated Ag^+ with surfactant/polymer, which offers the possibility of selective detection of Ag^+. With SDS and PVA-Vac stabilized emulsions, the linear dynamic detection ranges for Ag^+ detection are 50−175 and 24−124 ppb, respectively. The possible mechanisms of interaction of Ag^+ with surfactant and polymer are discussed. Our results offer promising practical applications for the selective detection of Ag^+ with high sensitivity using stimuli-responsive nanoemulsions.

■ ASSOCIATED CONTENT

Supporting Information

XRD, VSM, FTIR, TGA, hydrodynamic size distribution, and TEM of the Fe_3O_4 nanoparticles (Figure S1a−f); block diagram of the force measurement setup (Figure S2); the cryo-freeze fracture TEM images of two nanoemulsion droplets (Figure S3); the phase contrast optical microscopic images of these droplets (a) without and (b−f) with magnetic field show Brownian droplets and aligned droplets in 1-D, respectively (Figure S4); Bragg peak at different time intervals (Figure S5); schematic representation of three possible modes of Ag^+−SDS interaction (Figure S6); and variation of surface potential for 0.8 mM SDS stabilized emulsion with different Ag^+ concentrations (calculated from the fit to the force−distance curve) (Table St1). This material is available free of charge via the Internet at http://pubs.acs.org.

■ AUTHOR INFORMATION

Corresponding Author

*E-mail philip@igcar.gov.in; Fax 00 91-44-27450356; Tel 00 91 44 27480232 (J.P.).

Notes

The authors declare no competing financial interest.

■ ACKNOWLEDGMENTS

The authors thank Dr. T. Jayakumar and Dr. P. R. Vasudeva Rao for fruitful discussions. J.P. thanks the Board of Research Nuclear Sciences (BRNS) for support through a research grant for the advanced nanofluid development program.

■ REFERENCES

(1) Russel, W. B.; Saville, D. A.; Schowalter, W. R. *Colloidal Dispersions*; Cambridge University Press: New York, 1989.

(2) Baimpos, T.; Shrestha, B. R.; Raman, S.; Valtiner, M. Effect of interfacial ion structuring on range and magnitude of electric double layer, hydration, and adhesive interactions between mica surfaces in 0.05−3M Li^+ and Cs^+ electrolyte solutions. *Langmuir* **2014**, *30*, 4322−4332.

(3) Manor, O.; Chau, T. T.; Stevens, G. W.; Chan, D. Y. C.; Grieser, F.; Dagastine, R. R. Polymeric stabilized emulsions: Steric effects and deformation in soft systems. *Langmuir* **2012**, *28*, 4599−4604.

(4) Owen, R. J.; Crocker, J. C.; Verma, R.; Yodh, A. G. Measurement of long-range steric repulsions between microspheres due to an adsorbed polymer. *Phys. Rev. E* **2001**, *64*, 011401−011406.

(5) Murakami, R.; Binks, B. P.; Moriyama, H.; Yamamoto, M.; Rocher, A. Particle stabilization of oil-in-water-in-air materials. *Adv. Mater.* **2012**, *24*, 767−771.

(6) Aveyard, R.; Binks, B. P.; Esquena, J.; Fletcher, P. D. I.; Bault, P.; Villa, P. Flocculation transitions of weakly charged oil-in-water emulsions stabilized by different surfactants. *Langmuir* **2002**, *18*, 3487−3494.

(7) Braem, A. D.; Prieve, D. C.; Tilton, R. D. Electrostatically tunable coadsorption of sodium dodecyl sulfate and poly(ethylene oxide)-b-poly(propylene oxide)-b-poly(ethylene oxide) triblock copolymer to silica. *Langmuir* **2001**, *17*, 883−890.

(8) Tulpar, A.; Tilton, R. D.; Walz, J. Y. Synergistic effects of polymers and surfactants on depletion forces. *Langmuir* **2007**, *23*, 4351−4357.

(9) Philip, J.; Gnanaprakash, G.; Jayakumar, T.; Kalyanasundaram, P.; Raj, B. Three distinct scenarios under polymer, surfactant, and colloidal interaction. *Macromolecules* **2003**, *36*, 9230−9236.

(10) Sakata, S.; Inoue, Y.; Ishihara, K. Quantitative evaluation of interaction force between functional groups in protein and polymer brush surfaces. *Langmuir* **2014**, *30*, 2745−2751.

(11) Lopez-Lopez, M. T.; Zubarevb, A. Y.; Bossis, G. Repulsive force between two attractive dipoles, mediated by nanoparticles inside a ferrofluid. *Soft Matter* **2010**, *6*, 4346.

(12) Eberle, A. P. R.; Wagner, N. J.; Castaneda-Priego, R. Dynamical arrest transition in nanoparticle dispersions with short range interactions. *Phys. Rev. Lett.* **2011**, *106*, 105704.

(13) Israelachvili, J. N.; Tandor, R. K.; White, L. R. Measurement of forces between two mica surfaces in aqueous poly(ethylene oxide) solutions. *Nature* **1979**, *277*, 120−121.

(14) Klien, J. Forces between mica surfaces bearing layers of adsorbed polystyrene in cyclohexane. *Nature* **1980**, *288*, 248−250.

(15) Leal-Calderon, F.; Stora, T.; Mondain Monval, O.; Bibette, J. Direct measurement of colloidal forces. *Phys. Rev. Lett.* **1994**, *72*, 2959.

(16) Velegol, D.; Anderson, J. L.; Garoff, S. Determining the forces between polystyrene latex spheres using differential electrophoresis. *Langmuir* **1996**, *12*, 4103−4110.
(17) Bevan, M. A.; Prieve, D. C. Forces and hydrodynamic interactions between polystyrene surfaces with adsorbed PEO−PPO−PEO. *Langmuir* **2000**, *16*, 9274−9281.
(18) Tadros, T. Interaction forces between particles containing grafted or adsorbed polymer layers. *Adv. Colloid Interface Sci.* **2003**, *104*, 191−226.
(19) Dagastine, R. R.; Stevens, G. W.; Chan, D. Y. C.; Grieser, F. Forces between two oil drops in aqueous solution measured by AFM. *J. Colloid Interface Sci.* **2004**, *273*, 339−342.
(20) Lokar, W. J.; Ducker, W. A. Forces between glass surfaces in mixed cationic-zwitterionic surfactant systems. *Langmuir* **2004**, *20*, 4553.
(21) Park, B. J.; Pantina, J. P.; Furst, E. M.; Oettel, M.; Reynaert, S.; Vermant, J. Direct measurements of the effects of salt and surfactant on interaction forces between colloidal particles at water-oil interfaces. *Langmuir* **2008**, *24*, 1686−1694.
(22) Drechsler, A.; Synytska, A.; Uhlmann, P.; Elmahdy, M. M.; Stamm, M.; Kremer, F. Interaction forces between microsized silica particles and weak polyelectrolyte brushes at varying pH and salt concentration. *Langmuir* **2010**, *26*, 6400−6410.
(23) Pu, S.; Chen, X.; Chen, L.; Liao, W.; Chen, Y.; Xia, Y. Tunable magnetic fluid grating by applying a magnetic field. *Appl. Phys. Lett.* **2005**, *87*, 021901.
(24) López-López, M. T.; Gómez-Ramírez, A.; Rodríguez-Arco, L.; Durán, J. D. G.; Iskakova, L.; Zubarev, A. Colloids on the frontier of ferrofluids. Rheological properties. *Langmuir* **2012**, *28*, 6232−6245.
(25) Philip, J.; Jaykumar, T.; Kalyanasundaram, P.; Raj, B. A tunable optical filter. *Meas. Sci. Technol.* **2003**, *14*, 1289−1294.
(26) Park, B. J.; Fang, F. F.; Choi, H. J. Magnetorheology: materials and application. *Soft Matter* **2010**, *6*, 5246−5253.
(27) Kim, Y. J.; Liu, Y. D.; Seo, Y.; Choi, H. J. Pickering-emulsion-polymerizes polystyrene/Fe_2O_3 composite particles and their magnetoresponsive characteristics. *Langmuir* **2013**, *29*, 4959−4965.
(28) Sun, K.; Kumar, R.; Falvey, D. E.; Raghavan, S. R. Photogelling colloidal dispersions based on light-activated assembly of nanoparticles. *J. Am. Chem. Soc.* **2009**, *131*, 7135−7141.
(29) Philip, J.; Mondain-Monval, O.; Leal-Calderon, F.; Bibette, J. Colloidal force measurements in the presence of a polyelectrolyte. *J. Phys. D: Appl. Phys.* **1997**, *30*, 2798.
(30) Espert, A.; Omerjee, P.; Bibette, J.; Leal-Calderon, F.; Mondain Monval, O. Forces between liquid interfaces in the presence of polymer: Concentration, solvent, and mass effects. *Macromolecules* **1998**, *31*, 7023−7029.
(31) Lyklema, J.; Vliet, T. V. Polymer-stabilized free liquid films. *Faraday Discuss. Chem. Soc.* **1978**, *65*, 25−32.
(32) Sotiriou, G. A.; Meyer, A.; Knijnenburg, J. T. N.; Panke, S.; Pratsinis, S. E. Quantifying the origin of released Ag^+ ions from nanosilver. *Langmuir* **2012**, *28*, 15929−15936.
(33) A Lemire, J.; J Harrison, J.; J Turner, R. Antimicrobial activity of metals: mechanisms, molecular targets and applications. *Nat. Rev. Microbiol.* **2013**, *11*, 371−384.
(34) Ratte, H. T. Bioaccumulation and toxicity of silver compounds: A review. *Environ. Toxicol. Chem.* **1999**, *18*, 89−108.
(35) Chernousova, S.; Epple, M. Silver as antibacterial agent: Ion, nanoparticle, and metal. *Angew. Chem., Int. Ed.* **2013**, *52*, 1636−1653.
(36) Mondain-Monval, O.; Espert, A.; Omarjee, P.; Bibette, J.; Leal-Calderon, F.; Philip, J.; Joanny, J. F. Polymer-induced repulsive forces: Exponential scaling. *Phys. Rev. Lett.* **1998**, *80*, 1778−1781.
(37) Philip, J.; Gnanaprakash, G.; Jaykumar, T.; Kalyanasundaram, P.; Mondain-Monval, O.; Raj, B. Interaction between emulsion droplets in the presence of polymer−surfactant complexes. *Langmuir* **2002**, *18*, 4625.
(38) Shima, P. D.; Philip, J.; Raj, B. Synthesis of aqueous and nonaqueous iron oxide nanofluids and study of temperature dependence on thermal conductivity and viscosity. *J. Phys. Chem. C* **2010**, *114*, 18825−18833.
(39) Bibette, J. Depletion interactions and fractionated crystallization for polydisperse emulsion purification. *J. Colloid Interface Sci.* **1991**, *147*, 474−478.
(40) Philip, J.; Jaykumar, T.; Kalyanasundaram, P.; Raj, B.; Monval, O. M. Effect of polymer-surfactant association on colloidal force. *Phys. Rev. E* **2002**, *66*, 011406.
(41) Liu, J.; Lawrence, E. M.; Wu, A.; Ivey, M. L.; Flores, G. A.; Javier, K.; Bibette, J.; Richard, J. Field-induced structures in ferrofluid emulsions. *Phys. Rev. Lett.* **1995**, *74*, 2828−2831.
(42) Yang, Y.; Gao, L.; Lopez, G. P.; Yellen, B. B. Tunable assembly of colloidal crystal alloys using magnetic nanoparticle fluids. *ACS Nano* **2013**, *7*, 2705−2716.
(43) Tobias, D. J.; Hemminger, J. C. Getting specific about specific ion effects. *Science* **2008**, *319*, 1197−1199.
(44) Hofmeister, F. Zur Lehre von der Wirkung der Salze. *Arch. Exp. Pathol. Pharmakol.* **1888**, *24*, 247−260.
(45) Nostro, P. L.; Ninham, B. W. Hofmeister phenomena: An update on ion specificity in biology. *Chem. Rev.* **2012**, *112*, 2286−2322.
(46) Merat, K.; Chaodamrongsakul, J.; Tanthanuch, W.; Vao-soongnern, V. Atomistic solvation structure of calcium ion in poly(vinyl alcohol) as studied by molecular dynamics simulation and X-ray absorption spectroscopy. *J. Non-Cryst. Solids* **2013**, *371-372*, 47−52.
(47) Hamaker, H. C. The London-van der Waals attraction between spherical particles. *Physica* **1937**, *4*, 1058−1071.
(48) Hunter, R. J. *Zeta Potential in Colloid Science: Principles and Applications*; Academic Press: London, 1981.
(49) Israelachvili, J. N. *Intermolecular and Surface Forces*; Academic Press: San Diego, 1985.
(50) Pearson, R. G. Acids and bases. *Science* **1966**, *151*, 172−177.
(51) Gennes, P. G. D. Polymers at an interface. 2. Interaction between two plates carrying adsorbed polymer layers. *Macromolecules* **1982**, 492−500.
(52) Gennes, P. G. D. Dynamics of entangled polymer solutions. 1. The Rouse model. *Macromolecules* **1976**, *9*, 587−593.
(53) Zhang, H.; Zeeb, B.; Salminen, H.; Feng, F.; Weiss, J. Solubilization of octane in electrostatically-formed surfactant−polymer complexes. *J. Colloid Interface Sci.* **2014**, *417*, 9−17.
(54) Kim, J.; Gao, Y.; Hebebrand, C.; Peirtsegaele, E.; Helgeson, M. E. Polymer-surfactant complexation as a generic route to responsive viscoelastic nanoemulsions. *Soft Matter* **2013**, *9*, 6897−6910.
(55) Klein, J.; Rossi, G. Analysis of the experimental implications of the scaling theory of polymer adsorption. *Macromolecules* **1998**, *31*, 1979−1988.
(56) Skerjanc, J.; Kogej, K.; Vesnaver, G. Polyelectrolyte-surfactant interactions: enthalpy of binding of dodecyl- and cetylpyridinium cations to poly(styrenesulfonate) anion. *J. Phys. Chem.* **1988**, *92*, 6382−6385.
(57) Lutter, J. C.; Wu, T.-Y.; Zhang, Y. Hydration of cations: A key to understanding of specific cation effects on aggregation behaviors of PEO-PPO-PEO triblock copolymers. *J. Phys. Chem. B* **2013**, *117*, 10132−10141.
(58) Marcus, Y. A simple empirical model describing the thermodynamics of hydration of ions of widely varying charges, sizes, and shapes. *Biophys. Chem.* **1994**, *51*, 111−127.
(59) Yang, L.; Fan, Y.; Gao, Y. Q. Differences of cations and anions: Their hydration, surface adsorption, and impact on water dynamics. *J. Phys. Chem. B* **2011**, *115*, 12456−12465.